Science of the Total Environment 758 (2021) 143709

Contents lists available at ScienceDirect

Science of the Total Environment

journal homepage: www.elsevier.com/locate/scitotenv

Enhanced photochemical formation of secondary organic aerosols during the COVID-19 lockdown in Northern China

Jingjing Meng [a], Zheng Li [a], Ruiwen Zhou [a], Min Chen [a], Yuanyuan Li [a], Yanan Yi [a], Zhijian Ding [b], Hongji Li [c], Li Yan [d], Zhanfang Hou [a], Gehui Wang [b,*]

[a] School of Environment and Planning, Liaocheng University, Liaocheng 252000, China
[b] Key Laboratory of Geographic Information Science of the Ministry of Education, School of Geographic Sciences, East China Normal University, Shanghai 200062, China
[c] College of Environmental Science and Engineering, Jilin Normal University, Siping 136000, China
[d] Chinese Academy for Environmental Planning, Beijing 100012, China

HIGHLIGHTS

- The remarkable reductions in primary pollutant emissions during the lockdown
- Oxalic acid (C_2) and its precursors increased significantly during the lockdown
- The significant impact of biomass burning on C_2 before the lockdown
- The O_3-dominated formation pathways of C_2 during the lockdown

GRAPHICAL ABSTRACT

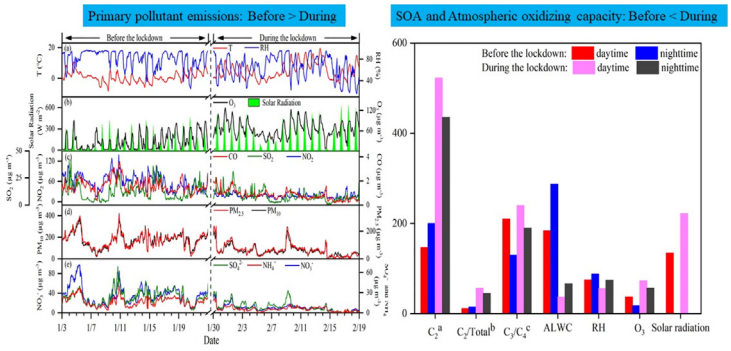

ARTICLE INFO

Article history:
Received 29 September 2020
Received in revised form 2 November 2020
Accepted 9 November 2020
Available online 14 November 2020

Editor: Pingqing Fu

Keywords:
Oxalic acid
Glyoxal and methyglyoxal
Ozone
Formation mechanisms
COVID-19 lockdown

ABSTRACT

To eliminate the spread of a novel coronavirus breaking out in the end of 2019 (COVID-19), the Chinese government has implemented a nationwide lockdown policy after the Chinese lunar New Year of 2020, resulting in a sharp reduction in air pollutant emissions. To investigate the impact of the lockdown on aerosol chemistry, the number fraction, size distribution and formation process of oxalic acid (C_2) containing particles and its precursors were studied using a single particle aerosol mass spectrometer (SPAMS) at the urban site of Liaocheng in the North China Plain (NCP). Our results showed that five air pollutants (i.e., $PM_{2.5}$, PM_{10}, SO_2, NO_2, and CO) decreased by 30.0–59.8% during the lockdown compared to those before the lockdown, while O_3 increased by 63.9% during the lockdown mainly due to the inefficient titration effect of O_3 via NO reduction. The increased O_3 concentration can boost the atmospheric oxidizing capacity and further enhance the formation of secondary organic aerosols, thereby significantly enhancing the C_2 particles and its precursors as observed during the lockdown. Before the lockdown, C_2 particles were significantly originated from biomass burning emissions and their subsequent aqueous-phase oxidation. The hourly variation patterns and correlation analysis before the lockdown suggested that relative humidity (RH) and aerosol liquid water content (ALWC) played a key role in the formation of C_2 particles and the increased aerosol acidity can promote the conversion of precursors such as glyoxal (Gly) and methyglyoxal (mGly) into C_2 particles in the aqueous phase. RH and ALWC decreased sharply but O_3 concentration and solar radiation increased remarkably during the lockdown, the O_3-dominated photochemical pathways played an important role in the formation of C_2 particles in which aerosol acidity was ineffective. Our study indicated that air pollution treatment sponges on a joint-control and balanced strategy for controlling numerous pollutants.

* Corresponding author.
E-mail addresses: ghwang@geo.ecnu.edu.cn, wanggh@ieecas.cn (G. Wang).

https://doi.org/10.1016/j.scitotenv.2020.143709
0048-9697/

1. Introduction

The outbreak of the novel coronavirus disease 2019 (COVID-19) has significantly impacted the world and become a substantial global threat to public health (Le et al., 2020; Wang et al., 2020a). To eliminate the spread of the virus among humans, the Chinese government first implemented effective regulatory policies such as urban lockdown, imposing traffic restrictions and suspending factory production, and required people to be quarantined at home beginning at the end of January 2020 (Chen et al., 2020). These restrictions make the Chinese air quality improve remarkably compared to the corresponding period in the past years (Li et al., 2020a; Shahzad et al., 2020). Five air pollutants in 44 cities of northern China including PM_{10}, $PM_{2.5}$, SO_2, NO_2, and CO decreased by 13.7%, 5.9%, 6.8%, 24.7%, and 4.6%, respectively, due to the travel restrictions during the COVID-19 pandemic (Bao and Zhang, 2020). However, a few severe haze events still occurred in China during the lockdown period in spite of a remarkable reduction in air pollutant emissions (Huang et al., 2020; Le et al., 2020). For example, model simulations and synergistic measurements have reported that the haze event during the COVID-19 lockdown was principally caused by increased aerosol heterogeneous reaction, stagnant airflow, together with fast secondary formation (Huang et al., 2020; Le et al., 2020; Li et al., 2020b). The enhanced secondary aerosols have been proposed as the dominant contributors to the haze pollution (Huang et al., 2020; Le et al., 2020). The remarkable reduction of NO_2 and $PM_{2.5}$ concentrations can lead to the enhancement of O_3, which can in turn improve the atmospheric oxidizing capacity and further promote the secondary organic aerosols (SOA) formation (Huang et al., 2020; Le et al., 2020; Li et al., 2020a; Xu et al., 2020b). However, the formation mechanism of increased SOA during the lockdown period is elusive especially at the molecular level.

Oxalic acid (C_2) and its precursors including glyoxal (Gly), methyglyoxal (mGly), glyoxylic acid (ωC_2), pyruvic acid (Pyr), and longer chain dicarboxylic acids ($C_{number} > 2$) have been regarded as significant SOA markers in the aerosol community (Meng et al., 2020). As the end product and the most abundant dicarboxylic acid, C_2 is omnipresent in cloud water, precipitation and wet particles because of its high water-soluble nature and low vapor pressure (Lin et al., 2020; Zhang et al., 2017). Therefore, C_2 plays a significant role in the hygroscopicity, acidity and cloud condensation nuclei (CCN) activity of atmospheric aerosols (Zhang et al., 2017). Although C_2 can be emitted directly from primary sources including biogenic activity, fossil fuel combustion, and biomass burning, C_2 is largely produced from the secondary oxidation of less oxygenated organic precursors such as Gly, mGly, ωC_2, and Pyr in the aqueous phase and the photochemical breakdown of longer chain diacids (Carlton et al., 2007; Fu et al., 2008; Meng et al., 2018; Myriokefalitakis et al., 2011; Wang et al., 2012; Zhang et al., 2019; Zhao et al., 2020). Moreover, the aqueous-phase photooxidation of large multifunctional compounds can also be a significant source of C_2 (Carlton et al., 2007). However, the formation mechanism of C_2 is still incompletely understood because of oxidant levels and other influencing factors such as aerosol acidity, aerosol liquid water content (ALWC) and meteorological parameters. Some studies proposed that the enhanced acidity might suppress the C_2 production during cloud processes (Sorooshian et al., 2007a, 2007b), but other studies claimed that more acidic conditions could promote the formation of C_2 and its precursors (Lin et al., 2020; Meng et al., 2020). Field observations revealed that the photochemical decomposition of Fe-C_2 complexes might result in the reduction of C_2 through forming acetic acid (Cheng et al., 2017; Passananti et al., 2016). However, other field measurements and laboratory experiments argued that the presence of Fe could boost the production of C_2 and its precursors due to Fe-driven Fenton reaction that can form OH radicals in liquid phase (Lin et al., 2018; Zhang et al., 2019). These controversies suggest the complexity of the formation mechanism of C_2. Thus, further investigations on the formation process of C_2 and related SOA are needed.

Online observations of the size distributions of C_2-containing particles and the mixing state of C_2 with other chemical species in single particles provide a useful tool to investigate the formation process of C_2 and its precursors (Cheng et al., 2017). The dramatical shutdown of pollutant emissions during the COVID-19 lockdown provides a natural experiment to assess the contribution of SOA in the atmosphere and to evaluate the impact of the emissions and the meteorological conditions on the formation mechanism of SOA. In this study we analyzed the number fraction, size distribution, mixing state and formation process of C_2 particles using a single particle aerosol mass spectrometer (SPAMS) before and during the lockdown to investigate the impact of emission controls on the chemistry of SOA in the urban region of Northern China.

2. Methods

2.1. Field measurements

Field measurements were performed at a national air quality monitoring station on the rooftop of a six-story building (36.43°N, 116.01°E; 25 m above ground) on the campus of Liaocheng University, which is situated in the southeast of Liaocheng (Fig. S1). Detailed information of the sampling site has been described elsewhere (Li et al., 2020b). Liaocheng is considered as one of the "2 + 26" air pollution transmission channel cities of China and located in the southwest of Shandong Province in the NCP. The sampling site is surrounded by main roads and residential communities, without significant industrial emissions or tall building nearby. Individual particles were collected hourly using the SPAMS (0515R Model, Hexin Analytical Instrument Co., Ltd., China) through a tygon tube of 3 m long at a flow rate of 75 $mL \cdot min^{-1}$. To explore the impact of COVID-19 lockdown on the formation mechanisms of oxalic acid (C_2)-containing particles, the whole observation period was divided into "before the lockdown" ranging from January 3 to 23 and "during the lockdown" ranging from January 23 to February 19 in 2020. Six air pollutants including PM_{10}, $PM_{2.5}$, SO_2, NO_x, CO and O_3, as well as meteorological parameters were obtained from the website of Environmental Protection Bureau of Liaocheng (http://www.lchbj.gov.cn).

2.2. Detection and classification of oxalate-containing particles

SPAMS was designed to determine the size distribution and chemical composition of ambient single particles at 1 h resolution. A detailed description has been described in previous studies (Li et al., 2020b; Yang et al., 2009). Based on (Cheng et al., 2017), oxalic acid (C_2) particles are identified if the peak area of m/z −89 was larger than 0.5% of the total signal in the negative mass spectrum. In the current work, 31,361 and 83,732 C_2 particles were obtained before and during the lockdown, respectively. In addition, the organic precursors of C_2 particles were queried by searching for given m/z ratios (Table 1) based on previous studies (Lin et al., 2020; Zhou et al., 2015).

Table 1
SPAMS markers used to search for the precursors of oxalic acid (C_2) containing particles.

	Species	m/z	Marker ion	Relative area peak	Function
α-Dicarbonyls	mGly	−71	$[C_3H_3O_2]^-$	>0.005	Not containing 113/115 $[K_2Cl]^+$ or 213/215 $[K_3SO_4]^+$ with a relative peak area of more than 0.5%.
	Gly	−73	$[C_2HO_3]^-$	>0.005	
Ketocarboxylic acids	ωC_2	−57	$[C_2HO_2]^-$	>0.005	
	Pyr	−87	$[C_3H_3O_3]^-$	>0.005	
Dicarboxylic acids	C_3	−103	$[C_3H_3O_4]^-$	>0.005	
	C_4	−117	$[C_4H_5O_4]^-$	>0.005	
	C_5	−131	$[C_5H_7O_4]^-$	>0.005	

The C_2 particles were categorized into five groups as follows: (1) C_2-biomass burning (BB), (2) C_2-secondary (Sec), (3) C_2-carbonaceous species (CS), (4) C_2-heavy metal (HM), and (5) C_2-other. Different types of particles were identified based on both the characteristic ion markers and predominant chemical species. Briefly, (1) particles containing strong signals of 39[K]$^+$ (peak area > 1500) with a relative peak area of −45[CHO_2]$^-$, −59[$C_2H_3O_2$]$^-$, −73[$C_3H_5O_2$]$^-$ and/or 113/115[K_2Cl]$^+$, 213/215[K_3SO_4]$^+$ higher than 0.5% are considered as C_2-BB type; (2) remaining particles containing abundant signals of 18[NH_4]$^+$ with peak area > 50, −62[NO_3]$^-$ and −97[HSO_4]$^-$ with peak area > 100 are considered as C_2-Sec type; (3) remaining particles containing abundant signals of carbon clusters (e.g., ±12[C]$^{+/-}$, ±24[C_2]$^{+/-}$, and ±36[C_3]$^{+/-}$) and/or hydrocarbon clusters (e.g., 27[C_2H_3]$^+$, 37[C_3H]$^+$, and 43[C_2H_3O]$^+$) with a relative peak area of higher than 0.5% are classified as C_2-CS type; (4) remaining particles containing signals of 55[Mn]$^+$, 56[Fe]$^+$, 63/65[Cu]$^+$, and 206/207/208[Pb]$^+$ with a relative peak area of more than 0.5% are classified as C_2-HM type; (5) remaining particles are classified as C_2-other type. The classification methods of C_2 particles in this study have been shown in previous studies (Cheng et al., 2017; Lin et al., 2020).

2.3. Aerosol liquid water content (ALWC) and in situ particle pH (pH_{is})

Water-soluble inorganic ions were measured hourly using an online analyzer (WARGA, Hangzhou Juguang Analytical Company) with a $PM_{2.5}$ sampling inlet during the whole observation period. Aerosol liquid water content (ALWC) and in situ particle pH (pH_{is}) in $PM_{2.5}$ samples were calculated using the ISORROPIA-II model, which treated the Na^+ - NH_4^+ - K^+ - Ca^{2+} - Mg^{2+} - SO_4^{2-} - NO_3^- - Cl^- system (Wu et al., 2018). The forward mode with a metastable state in the ISORROPIA model was employed.

3. Results and discussion

3.1. Variations in air quality and meteorological conditions

Temporal variations in the concentration of $PM_{2.5}$, PM_{10} and gaseous pollutants (e.g., SO_2, NO_2, O_3, and CO) along with meteorological parameters in the whole observation period are presented in Fig. 1. $PM_{2.5}$ and PM_{10} concentration were 63.8 ± 44.9 μg m^{-3} and 174 ± 67.2 μg m^{-3} during the lockdown, which decreased by 53.8% and 56.9% compared to those (138.2 ± 56.9 μg m^{-3} for $PM_{2.5}$, 75.1 ± 46.5 μg m^{-3} for PM_{10}) before the lockdown, reflecting that the air quality was significantly improved due to the dramatic reduction of pollutant emissions during the lockdown (Le et al., 2020; Li et al., 2020a). Similarly, the concentrations of SO_2, NO_2 and CO during the lockdown decreased by 30.0%, 69.8% and 50.0% than those before the lockdown. It is a remarkable fact that the drop of the NO_2 was the most prominent, which was also observed in other urban regions in the Yangtze River Delta Region (Li et al., 2020a) and Central China (Xu et al., 2020b), due to the drastic decrease of on-road vehicular traffic and industrial exhausts during the lockdown (Li et al., 2020a). On the contrary, the drop of the SO_2 was relatively smaller, which is attributed to the ongoing emissions from petrochemical facilities and power plants that cannot be shut down during the COVID-19 event (Le et al., 2020). O_3 is mainly originated from the photochemical formation of NO_x and volatile organic compounds (VOCs), thus it can be used to evaluate the atmospheric oxidation capacity (Fu et al., 2020). It is noteworthy that O_3 concentration (64.8 ± 23.6 μg m^{-3}) was 63.9% higher during the lockdown than that (27.5 ± 23.4 μg m^{-3}) before the lockdown, which was completely opposite to the variations of the other five air pollutants, suggesting the stronger atmospheric oxidation capacity during the lockdown. The formation of O_3 in the urban regions of China is mostly derived from NO_x (the sum of NO and NO_2)-saturated regime because of the scarce of HO_x radicals in the winter (Seinfeld and Pandis, 1998). Moreover, the sharp reduction of NO_2 concentration during the lockdown can lead to the lower concentration level of NO (Xu et al., 2020b), and then alleviated the titration of O_3 (Seinfeld and Pandis, 1998; Zou et al., 2019). Therefore, the sink of NO_2 can result in an enhancement of O_3 during the lockdown. Previous studies have demonstrated that the negative relationship between O_3 and $PM_{2.5}$ mass can be ascribed to the aerosol radiative effect on the photochemistry production of O_3 (Wu et al., 2020) and the decreased precursors of O_3 (Li et al., 2019). Moreover, the stronger solar radiation and higher temperature conditions during the lockdown (Fig. 1) were favorable for the formation and cumulation of O_3 (Xu et al., 2020b).

Secondary inorganic aerosols (SIA, i.e., SO_4^{2-}, NO_3^-, and NH_4^+) are major components of $PM_{2.5}$, which exhibited a similar pattern of variation with $PM_{2.5}$ mass (Fig. 1). SO_4^{2-}, NO_3^-, and NH_4^+ before the lockdown were 23.55 ± 10.2 μg m^{-3}, 36.2 ± 18.7 μg m^{-3}, and 17.1 ± 7.0 μg m^{-3},

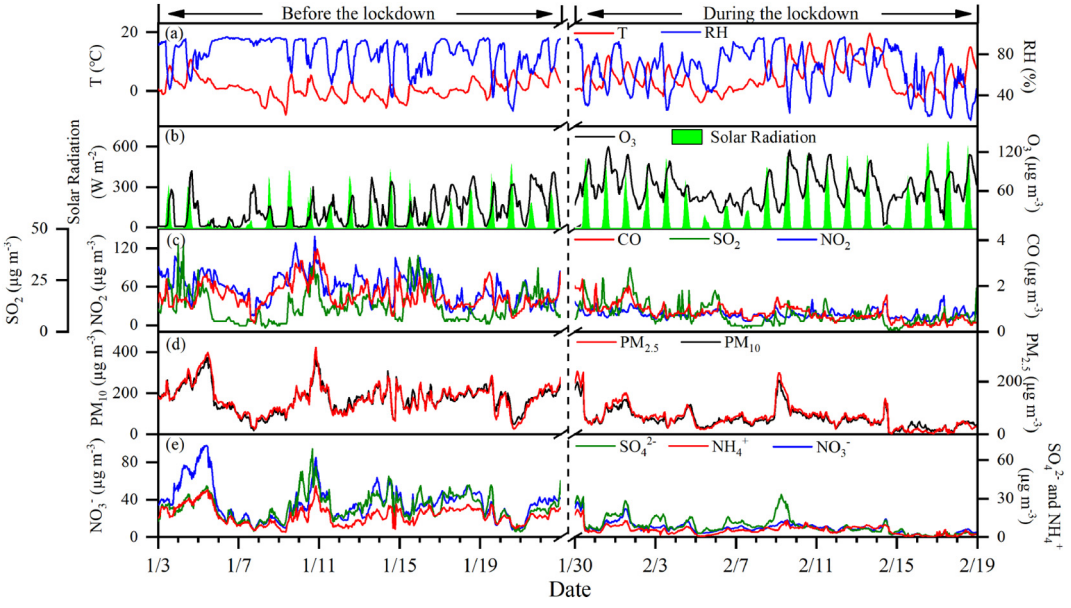

Fig. 1. Temporal variations of meteorological parameters and the concentrations of $PM_{2.5}$, PM_{10}, gaseous pollutants and major inorganic ions of $PM_{2.5}$ in the whole period.

accounting for 17.7, 26.2, and 13.0% of $PM_{2.5}$ mass, respectively. Their concentrations dropped to 8.8 ± 6.6 μg m^{-3}, 9.9 ± 6.0 μg m^{-3}, and 5.4 ± 3.5 μg m^{-3} during the lockdown with the contributions to $PM_{2.5}$ mass reduced to 14.6, 17.2, and 9.8%, respectively. Temperature increased dramatically from 0.8 ± 3.1 °C before the lockdown to 5.0 ± 5.2 °C during the lockdown, and solar radiation (242.0 ± 191.5 W m^{-2}) was much stronger during the lockdown than that (150.5 ± 133.6 W m^{-2}) before the lockdown. In contrast, relative humidity (RH) showed a decreasing trend, with an average of 81.4 ± 15.1% before the lockdown and 64.9 ± 20.7% during the lockdown. The ALWC is determined by SNA (Faust et al., 2017) and RH (Clegg et al., 1998). Both SNA concentrations and RH were higher before the lockdown compared to those during the lockdown, resulting in the ALWC before the lockdown (236 ± 190 μg m^{-3}) 4.6 times higher than that (52 ± 101 μg m^{-3}) during the lockdown. In contrast, pH_{is} increased from 0.9 ± 2.0 before the lockdown to 2.7 ± 2.1 during the lockdown, suggesting that the aerosols were less acidic during the lockdown than that before the lockdown.

3.2. The effect of lockdown on oxalic acid and its precursors

As shown in Fig. 2a and b, the number concentration of oxalic acid (C_2) particles increased markedly from 31,361 before the lockdown to 83,732 during the lockdown, accounting for 1.1 and 4.6% of the total number of detected particles, respectively. Thus, both the number concentration of C_2 particles and its percentage contribution of total particles (C_2/total) were higher during the lockdown than those before the lockdown, which could be ascribed to the enhanced secondary formation of C_2 particles during the lockdown (detailed discussions will be described in Sections 3.3 and 3.4). Similarly, the counts and percentages of the precursors of C_2 particles, including α-dicarbonyls (e.g., Gly and mGly), ketocarboxylic acids (e.g., ωC$_2$ and Pyr) as well as some longer chain dicarboxylic acids including malonic (C_3), succinic (C_4), and glutaric acids (C_5) were all higher during the lockdown than those before the lockdown (Fig. 2a and b), indicating an increased production of these precursors during the lockdown. Previous studies demonstrated that C_2 is an end product formed via photochemical oxidation of less oxygenated organic precursors including Gly, mGly, Pyr, and ωC$_2$ in wet aerosols or fog droplets and/or clouds, thus the ratios of C_2/Gly, C_2/mGly, C_2/ωC$_2$, and C_2/Pyr can be considered as key indicators to evaluate the aging degree of organic aerosols (Ervens et al., 2004a; Wang et al., 2012, 2015; Zhao et al., 2020). These four ratios all exhibited the bigger values during the lockdown than those before the lockdown (Fig. 2c), further demonstrating that the organic aerosols during the lockdown were more aged. It has been reported that large signals of secondary inorganic species (ammonium, nitrate, and sulfate) or the more intense signals of nitrate than sulfate in the same mass spectrum could be defined as aged particles (Moffet et al., 2008; Yang et al., 2009). The peak areas of m/z 18$[NH_4]^+$, −62$[NO_3]^-$ and −97$[HSO_4]^-$ represent ammonium, nitrate and sulfate, respectively. The mass spectrum of C_2 particles were characterized by strong signals of secondary inorganic species as well as more intense signals of nitrate than sulfate both before and during the lockdown, suggesting C_2 particles undergone an aging process during the whole period (Fig. 3). Moreover, the stronger signal intensity of secondary inorganic species during the lockdown than before the lockdown revealed the more aged C_2 particles during the lockdown (Fig. 3).

Previous studies have reported that C_4 can be photochemical degraded to C_3 in the atmosphere, thus the C_3/C_4 ratio can be proposed as a key marker to assess the photochemical production of SOA (Kawamura and Ikushima, 1993; Meng et al., 2020). The higher C_3/C_4 ratios during the lockdown (day: 2.4; night: 1.9) were observed than those (day: 2.1; night: 1.3) before the lockdown (Fig. 2c), which further suggested the more photochemical formation of SOA during the lockdown due to the stronger solar radiation and higher O_3 concentration.

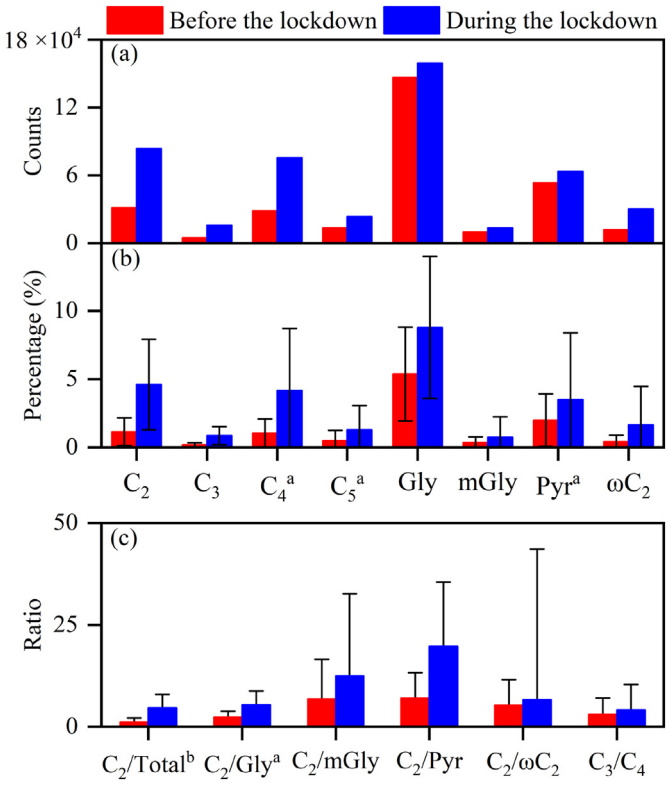

Fig. 2. Differences in (a) the counts of oxalic acid (C_2) containing particles and its precursors, (b) the relative abundance of C_2 particles and its precursors in the total detected particles, (c) major ratios of C_2 particles to total detected particles or its major precursors between before the lockdown and during the lockdown ([a]exaggerated by 10 times; [b]exaggerated by100 times).

As shown in Fig. 4, the C_2-BB particles made up as high as 38.3% of the total C_2 particles, followed by C_2-CS (24.2%) and C_2-Sec particles (19.8%) before the lockdown. It's worth noting that total C_2 particles exhibited a similar diurnal pattern with BB particles before the lockdown, indicating that BB was a significant source of C_2 particles. However, the contribution of C_2-BB particles decreased significantly to only 12% during the lockdown, when the C_2-Sec particles were the most abundant and contributed 35.4% to total C_2 particles during the lockdown, followed by CS (25.6%) and HM (17.8%) particles. During the lockdown, total C_2 particles and HM particles presented very similar diurnal patterns of variation (Fig. 4b), reflecting that the possible formation of C_2 particles was closely related to the transition metals such as Fe and Cu (Cheng et al., 2017; Zhou et al., 2015). Interestingly, the contribution of C_2-BB particles before the lockdown was 3.2 times higher than that during the lockdown, mainly because large amounts of organic compounds serving as precursors for C_2 particles emitted from BB decreased substantially due to the shutdown of power plants that use biomass as fuel in Liaocheng and its surrounding regions. Instead, all the electricity was mad by power plants, resulting in the percentage of C_2-EC particles during the lockdown increased by 2.1 times compared to that before the lockdown (Le et al., 2020; Li et al., 2020b).

The different peak modes suggest a heterogeneity in the atmospheric evolution process of C_2 particles (Cheng et al., 2017). The unscaled size distribution of C_2 particles mainly exists in the range of 0.4 to 1.5 μm with similar size distribution during the day and night especially in the larger size of 0.8 μm in the whole sampling period, but exhibited different peak modes before and during the lockdown (Fig. 5a). The number fraction of C_2 particles peaked at ~0.5 μm with a range of 0.4 to 1.3 μm before the lockdown. However, C_2 particles presented broader size mode from 0.4 to 1.5 μm and peaked at the larger size of ~0.8 μm during the lockdown than that before the lockdown, possibly attributed

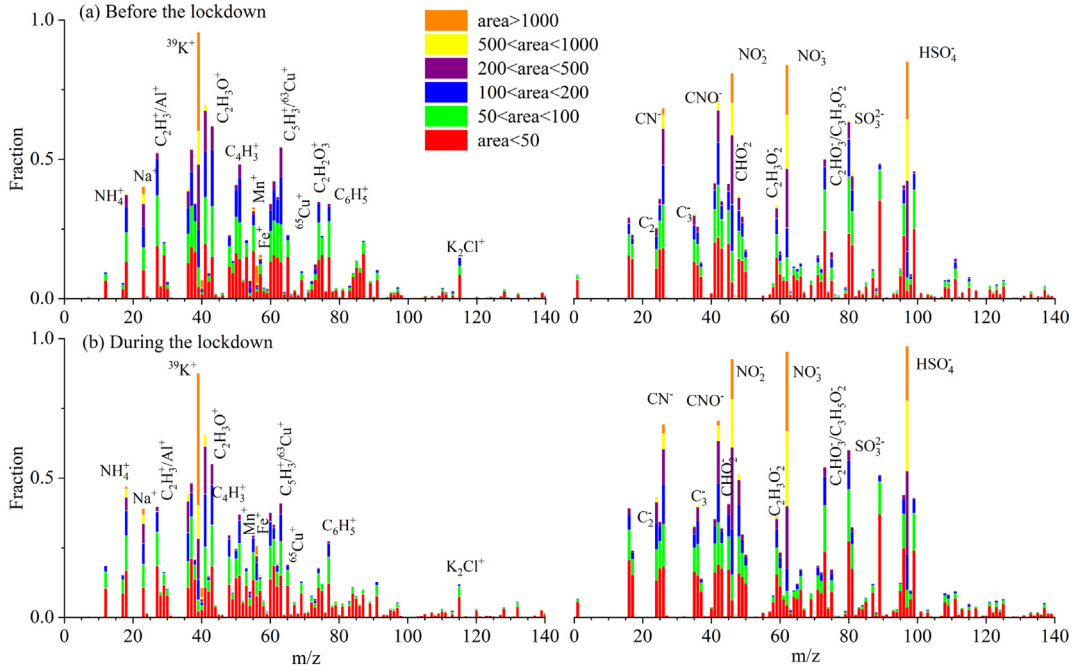

Fig. 3. The average positive and negative ion mass spectra of oxalic acid (C_2) containing particles (a) before the lockdown, (b) during the lockdown. Color bars represent each peak area corresponding to a specific fraction in individual particles.

to the condensation and coagulation of C_2 particles while aging during the lockdown (Zhang et al., 2017). In addition, the higher percentage contribution of C_2 particles to the total detected particles was another important explanation for the larger size of C_2 particles during the lockdown (Huang et al., 2019). Therefore, the particles during the lockdown can be considered to be more aged than those before the lockdown. The increase in the temperature was favorable for the formation of C_2 particles and its precursors (Meng et al., 2018). However, the higher temperature could increase the volatilization of oxalic acid, resulting in the decrease of oxalic acid in the particulate phase (Bilde et al., 2015). Therefore, there was no any correlation ($R^2 < 0.2$) between C_2 particles and temperature before and during the lockdown, respectively,

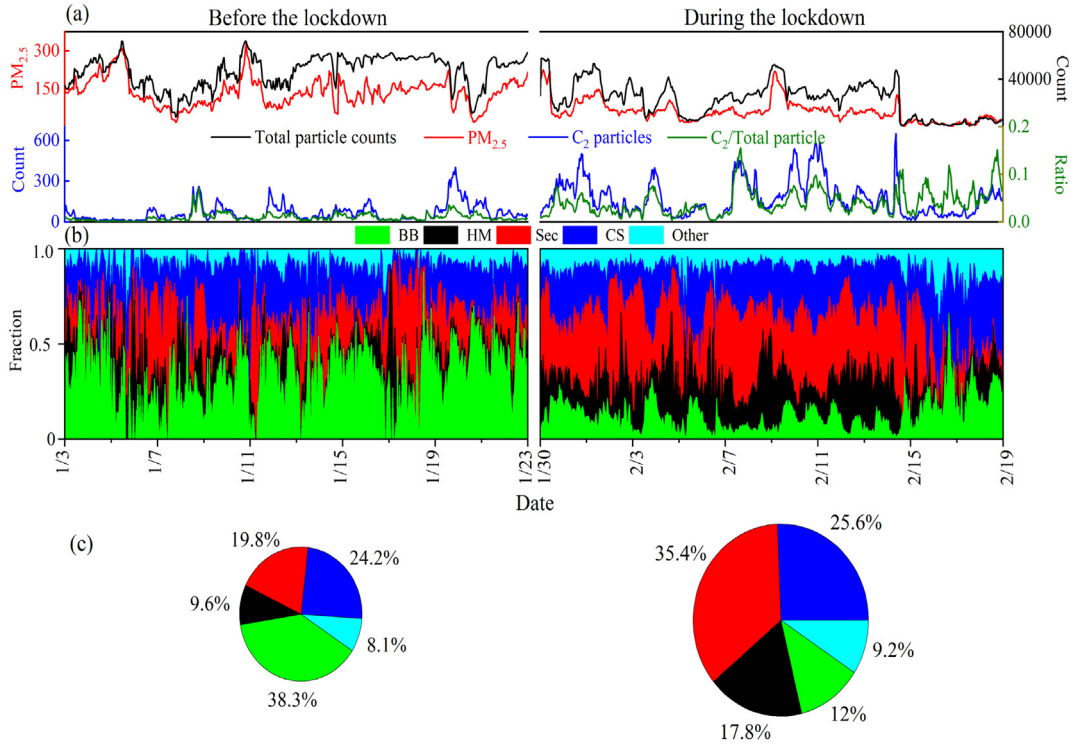

Fig. 4. (a) Hourly variations in total particle counts, $PM_{2.5}$ mass, oxalic acid (C_2) containing particles and the ratio of C_2 particles/total particles; (b) temporal variations in the fractions of five kinds of C_2 particles; (c) average percentages of five kinds of C_2 particles in the whole period.

suggesting that the temperature was a minor contributor to the formation of C_2 particles in this study.

3.3. Aqueous phase production of oxalic acid particles before the lockdown

Primary emissions from BB contribute only a negligible fraction to atmospheric C_2 particles (Meng et al., 2013; Yang et al., 2009). There is a growing consensus on the significance of C_2 particles from biomass burning particles through aqueous-phase oxidation according to field measurements (Cheng et al., 2017; Wang et al., 2020b; Xu et al., 2020a; Zhu et al., 2018). The positive mass spectrum of C_2 particles was characterized by a strong intensity of BB markers (e.g., $115K_2Cl^+$), as well as carbonaceous species such as $27C_2H_3^+$, $43C_2H_3O^+$, $51C_4H_3^+$, $74C_2H_2O_3^+$, and $77C_6H_5^+$, while the negative mass spectrum was dominated by secondary species (e.g., $46NO_2^-$, $62NO_3^-$, and $97HSO_4^-$), organic nitrogen ($26CN^-$ and $42CNO^-$) and levoglucosan ($45CHO_2^-$, $59C_2H_3O_2^-$, $73C_3H_5O_2^-$) before the lockdown (Fig. 3a). The higher fractions of BB markers and secondary species in the mass spectrum of C_2 particles might imply the significant contribution of BB and subsequent secondary formation to C_2 particles (Bi et al., 2011; Yang et al., 2009). Moreover, the relatively high contribution (38.3%) of C_2-BB particles to total C_2 particles (Fig. 4c) further highlighted the vitally significant impact of BB on the formation of C_2 particles before the lockdown. The number of C_2 particles in the night was both higher than those in the day (Fig. S2). One may expect that the higher number of C_2 particles was ascribed to the descended height of the boundary layer during the night. However, the higher ratio of C_2/total suggested that the lowered height of the boundary layer at night was not the reason (Cheng et al., 2015; Miyazaki et al., 2009). Based on the higher ALWC and RH in the night as well as the diurnal characteristic of C_2 particles (Fig. S2), we proposed that the higher number and percentage of C_2 particles at night may be associated with the enhanced production of C_2 through aqueous phase reactions. The linear correlation between C_2 particles and sulfate particles is generally ascribed to the aqueous-phase formation of C_2 particle (Wang et al., 2012; Yu et al., 2005). C_2 particles displayed strong correlations with sulfate particles ($R^2 = 0.75$, Fig. 6) and both particles exhibited similar size distributions (Fig. 5) in the whole observation period, indicating that C_2 particles experienced the aqueous-phase formation process in the wet aerosols and in cloud.

To better understand the formation mechanism of C_2 particles before the lockdown, the relatively higher counts of C_2 particles and C_2/total ratio from 11 to 19 January of 2020 was defined as a typical haze event. It is interesting to note that such a haze period was characterized by relatively higher RH (>60%) and ALWC (>96.8 μg m^{-3}) as well as lower O_3 (<62.1 μg m^{-3}) and solar radiation (daytime: <228.1 wat m^{-2}), which not only facilitate the aqueous phase formation of C_2 particles but also alleviate the production via photochemical oxidation. The photochemical oxidation of biogenic and anthropogenic VOCs can generate water-soluble semi-volatile gaseous Gly and mGly, which partition into the aerosol enriched with ALWC, and ultimately produce C_2 via ωC_2 and Pyr (Ervens et al., 2004b; Kawamura et al., 2013; Lim et al., 2005). Higher RH and ALWC can accelerate gas-to-aerosol aqueous phase partitioning of Gly and mGly, thus RH and ALWC are fatal factors determining the formation of C_2 (Carlton et al., 2006; Meng et al., 2020). As shown in Fig. 7a, the numbers of C_2 and C_2/total ratio exhibited similar diurnal patterns of variations with RH and ALWC, with a smaller peak at 4:00 and a larger peak at 9:00, suggesting that the enhanced production was significantly determined by RH and ALWC. However, such similar variations were not obtained in the organic precursors such as Gly, mGly and C_3-C_5 diacids, which exhibited different variations with RH and ALWC (Fig. 7a). The ratio of relative peak area of C_2 particles to precursors in the same particles was used to assess the conversion of precursors to C_2 particles (Lin et al., 2020; Zhang et al., 2019). The ratios of C_2/Gly and C_2/mGly correlated well with RH and ALWC ($R^2 > 0.5$, Fig. 6), suggesting that the conversion of α-dicarbonyls to C_2 particles was influenced significantly by RH and ALWC.

The enhanced production of C_2 particles was not only associated with high RH and ALWC, but also closely related to the strong acidic environment (Jang et al., 2002; Lim et al., 2010; Meng et al., 2018). The SPAMS cannot provide aerosol acidity similar to the bulk mass technology because of transmission efficiencies, hit efficiency and matrix effect on data gathering (Lin et al., 2020). To better understand the impact of acidic condition on the formation of C_2 particles, relative aerosol acidity (R_{ra}) was defined as the ratio of total peak areas of sulfate and nitrate to that of ammonium (Denkenberger et al., 2007). R_{ra} is correlated strongly with pH_{is} calculated by the ISORROPIA-II model before ($R^2 = 0.62$, Fig. S3a) and during the lockdown ($R^2 = 0.62$, Fig. S3b), respectively, confirming the validity of R_{ra} estimated by the SPAMS. The higher R_{ra} (77.0 ± 20.1) of particles before the lockdown than during the lockdown (61.6 ± 16.0) implied that the aerosol particles before the lockdown was more acidic. The hourly variations of R_{ra} exhibited a similar pattern as the peak area of Gly and mGly (Fig. 7a), suggesting that the production of precursors of C_2 particles was closely associated with the enhanced R_{ra}. Laboratory experiment demonstrated that the uptake and formation of Gly and mGly could be promoted in acidic conditions

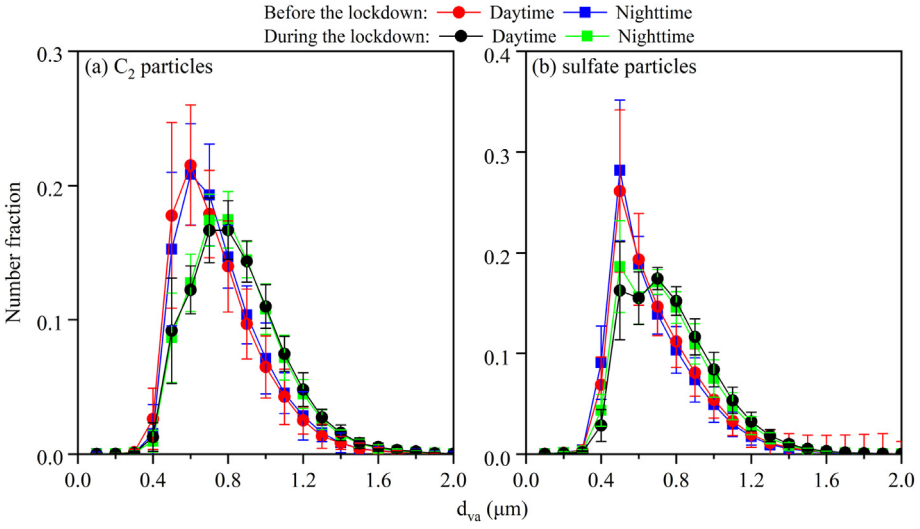

Fig. 5. Unscaled size distribution of (a) oxalic acid (C_2) containing particles and (b) sulfate particles during the sampling period.

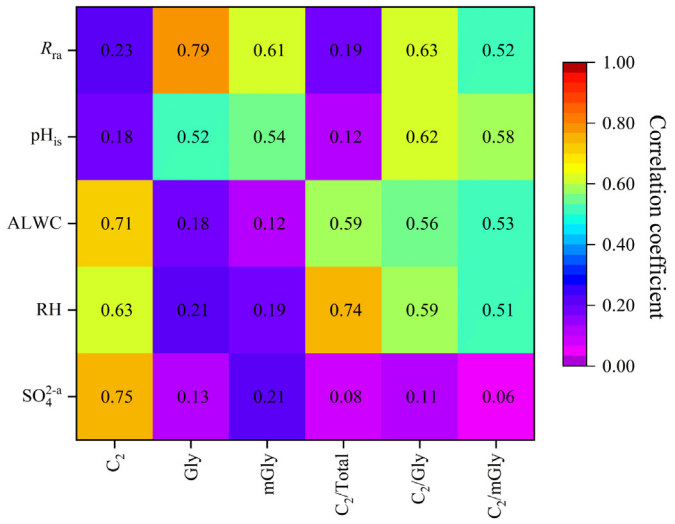

Fig. 6. Correlation coefficients (R^2) of numbers of oxalic acid (C_2), glyoxal (Gly) and methyglyoxal (mGly) containing particles as well as the ratios of C_2/total, C_2/Gly and C_2/mGly with the relative aerosol acidity (R_{ra}), in situ particle pH (pH$_{is}$), aerosol liquid water content (ALWC), relative humidity (RH) and sulfate particles (SO_4^{2-}) before the lockdown ([a]in the whole observation period).

through acidic-catalyzed heterogeneous reaction (Jang et al., 2002). However, the increased C_2 particles were not obtained with the enhanced R_{ra} (Fig. 7a), which was consistent with the measurements in the rural area of Pearl River Delta (Cheng et al., 2017) and Nanling background station (Lin et al., 2020) of China. The ratios of C_2/Gly ($R^2 > 0.6$, Fig. 6) and C_2/mGly ($R^2 > 0.5$, Fig. 6) are highly correlated with R_{ra} and pH$_{is}$, suggesting that the enhancement of aerosol acidity can promote the conversion of precursors to C_2 particles in the aqueous phase despite no correlation between C_2 particles and R_{ra} or pH$_{is}$ ($R^2 < 0.25$, Fig. 6).

3.4. O_3-dominated formation pathways of oxalic acid during the lockdown

O_3 (Yu et al., 2019) and solar radiation (Deshmukh et al., 2018) have been proposed as reliable indicators of photochemical oxidation in gaseous phase. The O3-dominated photochemical pathways are also proposed to be closely involved in the formation of C_2 particles from field observations (Meng et al., 2020; Mochizuki et al., 2017). Although the primary sources including biomass burning and coal combustion declined sharply, the higher number and percentage of C_2 particles were observed during the lockdown than before the lockdown (Fig. 2). Considering the remarkable enhancement of O_3 concentration and solar radiation during the lockdown discussed in Section 3.1, Figs. 1 and S2, the photochemical pathways could play significant roles in the formation of C_2 particles. In contrast to the diurnal variations before the lockdown, C_2 particles and C_2/total presented larger values in the day than those in the night (Fig. S2). The relatively higher O_3 concentration and the stronger solar radiation conditions in the daytime can promote the photochemical formation of α-dicarbonyls and other precursors from VOCs (Cheng et al., 2017; Myriokefalitakis et al., 2011), which further accelerated the formation of C_2 particles. As shown in Fig. S2, the number and percentage of C_2 particles exhibited similar pattern of variation with O_3 concentration. Moreover, it is interesting to note that the number of C_2 particles ($R^2 = 0.78$), C_2/total ($R^2 = 0.65$) and C_3/C_4 ratios ($R^2 = 0.52$) are correlated strongly with O_3 concentration and solar radiation (only from 9:00 to 18:00) ($R^2 > 0.65$) during the lockdown, which could be concluded that the O_3-dominated photochemical processing under the stronger solar radiation contributed substantially to the C_2 formation during the lockdown.

To investigate the photochemical pathways of C_2 particles and influencing factors during the lockdown, the hourly variations of C_2

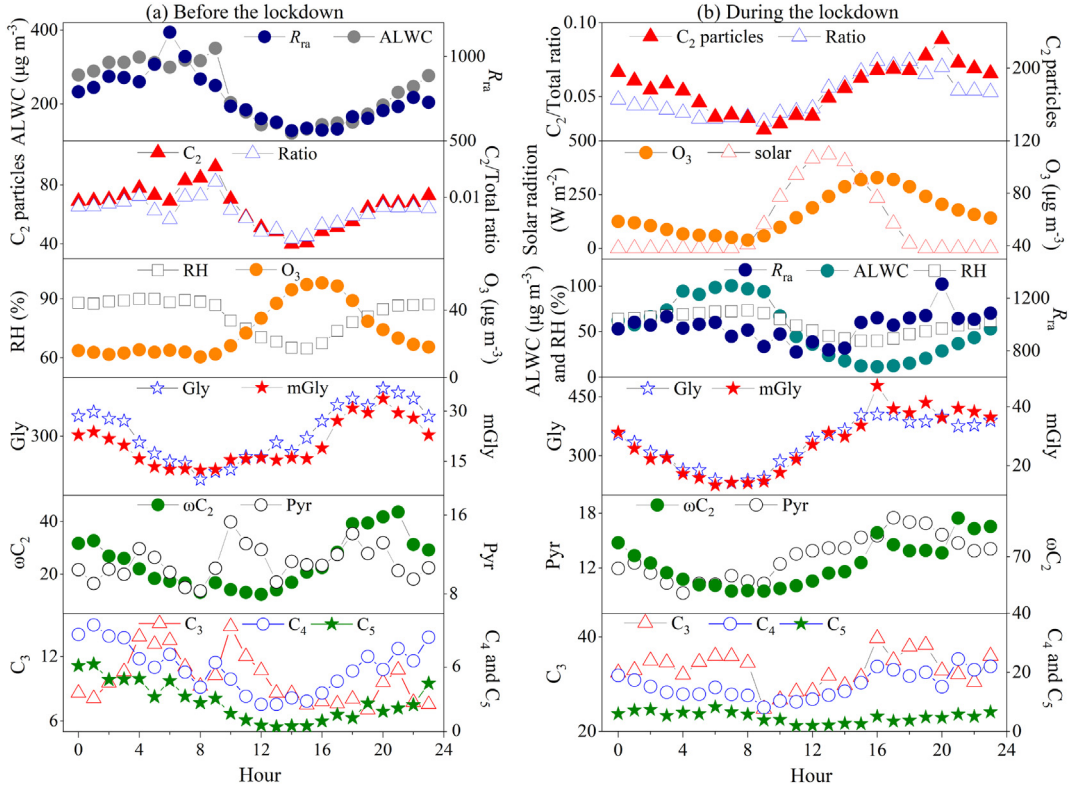

Fig. 7. Hourly variations in oxalic acid (C_2) containing particles and the ratio of C_2 particles to total detected particles (C_2/total ratio), major precursors of C_2 particles, the relative aerosol acidity (R_{ra}), aerosol liquid water content (ALWC) concentration, O_3 concentration and meteorological parameters (a) before the lockdown, (b) during the lockdown.

particles, the precursors (e.g., Gly, mGly, Pyr, ωC_2 and C_2-C_5 dicarboxylic acids), O_3, and physical parameters (ALWC and pH_{is}) averaged from 9 to 13 February during the lockdown were presented in Fig. 7b along with meteorological parameters (e.g., RH and solar radiation). The date from 9 to 13 February was characterized by higher concentration of O_3 and stronger solar radiation (Fig. 1). The O_3 concentration and solar radiation increased from 9:00 and showed a peak at 16:00, while C_2 particles and C_2/total ratio began to increase at 9:00 and reached a smaller peak at 15:00 and a bigger peak at 20:00 (Fig. 7b). The R_{ra} was relatively lower from 9:00 to 20:00 than that in other time (Fig. 7b), indicating a negligible impact of aerosol acidity on the photochemical formation of C_2 particles. If the ratios of C_2/C_4, C_3/C_4 and C_2/total detected diacids (sum of C_2-C_5 diacids) (C_2/TDAs) are correlated significantly with O_3, C_2 should be produced from the photochemical degradation of longer chain diacids (Kawamura and Ikushima, 1993; Zhao et al., 2020). Strong correlations were obtained between the ratios of C_2/C_4, C_3/C_4, C_2/TDAs and O_3 ($R^2 > 0.65$, Fig. 8) from 9:00 to 16:00 than those ($0.50 < R^2 < 0.56$, Fig. 7) from 16:00 to 20:00. In addition, higher correlations ($R^2 > 0.88$, Table 2) were also found between C_2 and longer chain diacids including C_3-C_5 diacids from 9:00 to 16:00 than those ($0.48 < R^2 < 0.56$, Table 2) from 16:00 to 20:00. The consumption rates of longer-chain diacids for producing C_2 has proven to be slower than their supply rates (Zhao et al., 2020). These findings implied that the photodegradation of longer chain diacids contributed more to the formation of C_2 particles from 9:00 to 16:00. As shown in Fig. 7b, RH and ALWC began to increase at 16:00 when C_2 particles and C_2/total ratio continued to rise and maximized at 20:00. Furthermore, C_2 particles and C_2/total ratio exhibited similar variations with RH and ALWC from 16:00 to 20:00, respectively, suggesting that RH and ALWC might play important roles in the C_2 particles formation during this period. Compared to longer chain diacids, close relationships were obtained between C_2 particles and other precursors, including Gly, mGly, ωC_2 and Pyr from 16:00 to 20:00 (Table 1). Modeling studies and field observations demonstrated that RH and ALWC are important factors determining the conversion of organic precursors to C_2 particles (Kunwar et al., 2019; Lin et al., 2020; Myriokefalitakis et al., 2011; Zhang et al., 2017). The more significant correlations of C_2 with Gly ($R^2 = 0.89$) and ωC_2 ($R^2 = 0.82$) than those of C_2 with mGly ($R^2 = 0.65$) and Pyr ($R^2 = 0.56$) from 16:00 to 20:00 were found (Table 1), largely because

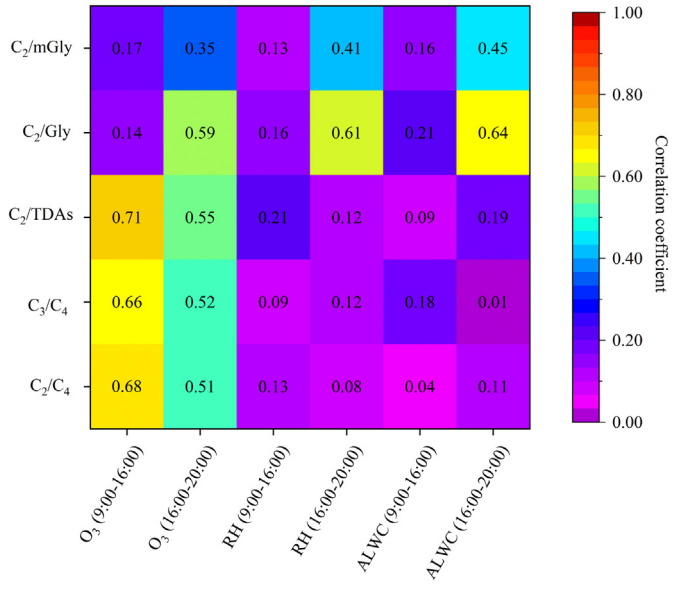

Fig. 8. Correlation coefficients (R^2) of the ratios of C_2/mGly, C_2/Gly, C_2/total numbers of C_2 to C_5 diacids (TDAs), C_3/C_4 and C_2/C_4 with O_3 concentration, the relative humidity (RH) and aerosol liquid water content (ALWC) from 9:00 to 16:00 and from 16:00 to 20:00 during the lockdown.

Table 2
Correlation coefficients (R^2) of the peak area of oxalic acid (C_2) containing particles with its precursors from 9:00 to 16:00 and from 16:00 to 20:00 during the lockdown.

	C_2 (9:00–16:00)	C_2 (16:00–20:00)
C_3	0.92	0.53
C_4	0.93	0.55
C_5	0.89	0.49
Gly	0.45	0.89
mGly	0.38	0.65
ωC_2	0.41	0.82
Pyr	0.36	0.56

the oxidation rate of mGly (1.1×10^9 M^{-1} s^{-1}) with OH radicals in the aqueous phase is lower than Gly (3×10^{10} M^{-1} s^{-1}) (Carlton et al., 2007). Furthermore, the C_2/Gly ratio is correlated strongly with RH, ALWC and O_3 ($0.58 < R^2 < 0.65$, Fig. 8), while C_2/mGly ratio is correlated moderately with RH, ALWC and O_3 ($0.34 < R^2 < 0.46$, Fig. 8). These findings suggested that the accelerated secondary formation of C_2 was dominantly from the aqueous photooxidation of Gly from 16:00 to 20:00 in which high RH and ALWC were key favorable factors. The above results may explain the smaller peak at 15:00 and the bigger peak at 20:00. After the culmination, C_2 particles and C_2/total began to decrease from 21:00 (Fig. 7b), suggesting that the formation of C_2 particles was overwhelmed by a removal via dry deposition or transport out of the sampling region (Kawamura and Yasui, 2005).

Modeling studies and field observations reported that the photochemical decomposition of Fe-oxalate complexes is regarded as a substantial loss of C_2 (Cheng et al., 2017; Weller et al., 2014; Zhang et al., 2019). Based on the highly abundant ion peaks of Fe in the positive spectrum of C_2 particles, the photolysis of Fe-oxalate complexes was expected to be a significant sink of C_2 particles. The mass concentration of C_2 and Fe (III) cannot be measured in this study by SPAMS, the diurnal variations in the peak areas of Fe and C_2 particles were employed to understand the role of Fe in the formation process of C_2 particles in the HM particles (Fig. 9). It is interesting to note that the variation patterns of peak area of C_2 particles were opposite to the peak area of iron from 9:00 to 20:00 (Fig. 9). Such a phenomenon was also observed in the rural area of Pearl River Delta of China, where an opposite pattern of variations of C_2 particles and iron occurred from 5:00 to 19:00 (Cheng et al., 2017). In addition, the peak area of Fe started to increase with a minimum at 2:00 while the peak area of C_2 particles started to decrease with a maximum at 2:00 accordingly (Fig. 9), which was in accordance with the diurnal variation arising from the nighttime production of Fe-oxalate complexes and subsequent photochemical decomposition

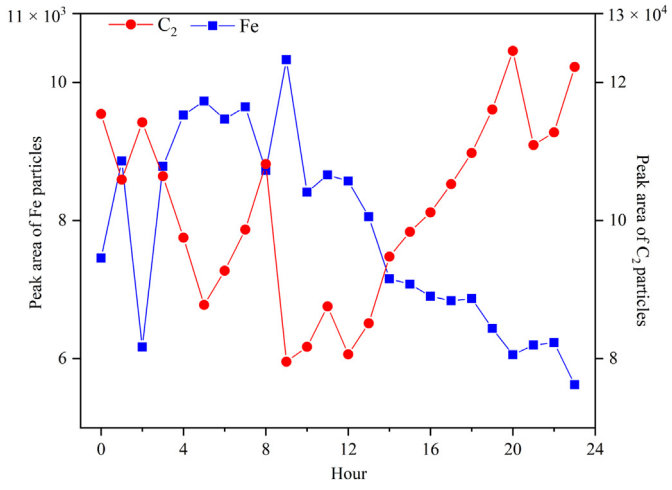

Fig. 9. Hourly variations in the peak area of Fe and oxalic acid (C_2) containing particles.

under solar radiation during the day. These results implied that the loss of C_2 particles via the photolysis of Fe-oxalate complexes was expected to be an efficient sink.

4. Summary and conclusions

Human activities decreased significantly during the COVID-19 lockdown, leading to significant reductions of the air pollutants including $PM_{2.5}$, PM_{10}, SO_2, NO_2, and CO. However, O_3 increased by 63.9% synchronously which in turn enhanced the atmospheric oxidizing capacity. The numbers and number fractions of C_2 particles and its precursors were higher during the lockdown compared to those before the lockdown, which suggested the enhanced formation of secondary organic species during the lockdown. Moreover, the higher ratios of C_2/total, C_2/Gly, C_2/mGly, $C_2/\omega C_2$ and C_2/Pyr as well as the more intense signals of secondary inorganic species (ammonium, nitrate, and sulfate) were observed during the lockdown than those before the lockdown, indicating that the aerosols during the lockdown were more aged. As high as 38.3% of C_2 particles contained biomass burning markers before the lockdown but dropped to only 9.3% during the lockdown due to the shut-down of power plants using biomass as fuel. Before the lockdown, the higher number and fractions of C_2 particles at night, the diurnal characteristic of C_2 particles as well as the strong correlations of C_2 particles with sulfate particles implied the substantial contribution of aqueous oxidation to C_2 particles production from Gly and mGly. The higher RH and ALWC, and the stronger aerosol acidity can favor the conversion of Gly and mGly to C_2 particles in the aqueous phase. The number and percentage of C_2 particles exhibited similar patterns of variation with O_3 concentration and solar radiation, suggesting that the O_3-dominated photochemical processing under the stronger solar radiation contributed substantially to the C_2 formation during the lockdown. The hourly variations of C_2 particles, the precursors (e.g., Gly, mGly, Pyr, ωC_2 and C_2-C_5 diacids) and O_3, along with correlation analysis revealed that the photodegradation of longer chain diacids contributed more to the formation of C_2 particles from 9:00 to 16:00 but the aqueous photooxidation of Gly contributed more to C_2 particles from 16:00 to 20:00 when high RH and ALWC were key favorable factors. The opposite diurnal variations in the peak area between Fe and C_2 particles indicated the loss of C_2 particles via the photolysis of Fe-oxalate complexes during the lockdown.

CRediT authorship contribution statement

GW designed and supervised the whole project. JM and ZL conducted the experiments and performed the data analyses. JM and GW wrote the manuscript. All authors contributed to the paper with useful scientific discussions or comments.

Declaration of competing interest

The authors declare that they have no known competing financial interests or personal relationships that could have appeared to influence the work reported in this paper.

Acknowledgements

This work was supported by China National Key Research and Development Program (Grant No. 2016YFC0207505), National Science Foundation of China (Grant Nos. 41505112 and 41702373) and Natural Science Foundation of Shandong Province (Grant No. BS2015HZ002).

Appendix A. Supplementary data

Supplementary data to this article can be found online at https://doi.org/10.1016/j.scitotenv.2020.143709.

References

Bao, R., Zhang, A., 2020. Does lockdown reduce air pollution? Evidence from 44 cities in northern China. Sci. Total Environ. 731, 139052.
Bi, X., Zhang, G., Li, L., Wang, X., Li, M., Sheng, G., et al., 2011. Mixing state of biomass burning particles by single particle aerosol mass spectrometer in the urban area of PRD, China. Atmos. Environ. 45, 3447–3453.
Bilde, M., Barsanti, K., Booth, M., Cappa, C.D., Donahue, N.M., Emanuelsson, E.U., et al., 2015. Saturation vapor pressures and transition enthalpies of low-volatility organic molecules of atmospheric relevance: from dicarboxylic acids to complex mixtures. Chem. Rev. 115, 4115–4156.
Carlton, A.G., Turpin, B.J., Lim, H.-J., Altieri, K.E., Seitzinger, S., 2006. Link between isoprene and secondary organic aerosol (SOA): pyruvic acid oxidation yields low volatility organic acids in clouds. Geophys. Res. Lett. 33, L06822.
Carlton, A.G., Turpin, B.J., Altieri, K.E., Seitzinger, S., Reff, A., Lim, H.-J., et al., 2007. Atmospheric oxalic acid and SOA production from glyoxal: results of aqueous photooxidation experiments. Atmos. Environ. 41, 7588–7602.
Chen, Q.-X., Huang, C.-L., Yuan, Y., Tan, H.-P., 2020. Influence of COVID-19 event on air quality and their association in Mainland China. Aerosol Air Qual. Res. 20, 1541–1551.
Cheng, C., Wang, G., Meng, J., Wang, Q., Cao, J., Li, J., et al., 2015. Size-resolved airborne particulate oxalic and related secondary organic aerosol species in the urban atmosphere of Chengdu, China. Atmos. Res. (161–162), 134–142.
Cheng, C., Li, M., Chan, C.K., Tong, H., Chen, C., Chen, D., et al., 2017. Mixing state of oxalic acid containing particles in the rural area of Pearl River Delta, China: implications for the formation mechanism of oxalic acid. Atmos. Chem. Phys. 17, 9519–9533.
Clegg, S.L., Brimblecombe, P., Wexler, A.S., 1998. Thermodynamic model of the system H+—NH4+—SO42-—NO3-—H2O at tropospheric temperatures. J. Phys. Chem. A 102, 2137–2154.
Denkenberger, K.A., Moffet, R.C., Holecek, J.C., Rebotier, T.P., Prather, K.A., 2007. Real-time, single-particle measurements of oligomers in aged ambient aerosol particles. Environmental Science & Technology 41, 5439–5446.
Deshmukh, D.K., Mozammel Haque, M., Kawamura, K., Kim, Y., 2018. Dicarboxylic acids, oxocarboxylic acids and α-dicarbonyls in fine aerosols over central Alaska: implications for sources and atmospheric processes. Atmos. Res. 202, 128–139.
Ervens, B., Feingold, G., Frost, G.J., Kreidenweis, S.M., 2004a. A modeling study of aqueous production of dicarboxylic acids: 1. Chemical pathways and speciated organic mass production. Journal of Geophysical Research: Atmospheres 109, D15205.
Ervens, B., Feingold, G., Frost, G.J., Kreidenweis, S.M., 2004b. A modeling study of aqueous production of dicarboxylic acids: 1. Chemical pathways and speciated organic mass production. J. Geophys. Res. 109, D15205.
Faust, J.A., Wong, J.P.S., Lee, A.K.Y., Abbatt, J.P.D., 2017. Role of aerosol liquid water in secondary organic aerosol formation from volatile organic compounds. Environmental Science & Technology 51, 1405–1413.
Fu, T.-M., Jacob, D.J., Wittrock, F., Burrows, J.P., Vrekoussis, M., Henze, D.K., 2008. Global budgets of atmospheric glyoxal and methylglyoxal, and implications for formation of secondary organic aerosols. J. Geophys. Res. 113, D15303.
Fu, X., Wang, T., Gao, J., Wang, P., Liu, Y., Wang, S., et al., 2020. Persistent heavy winter nitrate pollution driven by increased photochemical oxidants in Northern China. Environmental Science & Technology 54, 3881–3889.
Huang, X., Zhang, J., Luo, B., Luo, J., Zhang, W., Rao, Z., 2019. Characterization of oxalic acid-containing particles in summer and winter seasons in Chengdu, China. Atmos. Environ. 198, 133–141.
Huang, X., Ding, A., Gao, J., Zheng, B., Zhou, D., Qi, X., et al., 2020. Enhanced Secondary Pollution Offset Reduction of Primary Emissions During COVID-19 Lockdown in China.
Jang, M., Czoschke, N.M., Lee, S., Kamens, R.M., 2002. Heterogeneous atmospheric aerosol production by acid-catalyzed particle-phase reactions. Science 298, 814.
Kawamura, K., Ikushima, K., 1993. Seasonal changes in the distribution of dicarboxylic acids in the urban atmosphere. Environ Sci Technol 27.
Kawamura, K., Yasui, O., 2005. Diurnal changes in the distribution of dicarboxylic acids, ketocarboxylic acids and dicarbonyls in the urban Tokyo atmosphere. Atmos. Environ. 39, 1945–1960.
Kawamura, K., Tachibana, E., Okuzawa, K., Aggarwal, S.G., Kanaya, Y., Wang, Z.F., 2013. High abundances of water-soluble dicarboxylic acids, ketocarboxylic acids and α-dicarbonyls in the mountain aerosols over the North China Plain during wheat burning season. Atmos. Chem. Phys. 13, 3695–3734.
Kunwar, B., Kawamura, K., Fujiwara, S., Fu, P., Miyazaki, Y., Pokhrel, A., 2019. Dicarboxylic acids, oxocarboxylic acids and α-dicarbonyls in atmospheric aerosols from Mt. Fuji, Japan: implication for primary emission versus secondary formation. Atmos. Res. 221, 58–71.
Le, T., Wang, Y., Liu, L., Yang, J., Yung, Y.L., Li, G., et al., 2020. Unexpected air pollution with marked emission reductions during the COVID-19 outbreak in China. Science eabb7431.
Li, K., Jacob, D.J., Liao, H., Shen, L., Zhang, Q., Bates, K.H., 2019. Anthropogenic drivers of 2013–2017 trends in summer surface ozone in China. Proc. Natl. Acad. Sci. 116, 422.
Li, L., Li, Q., Huang, L., Wang, Q., Zhu, A., Xu, J., et al., 2020a. Air quality changes during the COVID-19 lockdown over the Yangtze River Delta Region: an insight into the impact of human activity pattern changes on air pollution variation. Sci. Total Environ. 732, 139282.
Li, Z., Meng, J., Zhou, L., Zhou, R., Fu, M., Wang, Y., et al., 2020b. Impact of the COVID-19 event on the characteristics of atmospheric single particle in the Northern China. Aerosol Air Qual. Res. 20, 1716–1726.
Lim, H.-J., Carlton, A.G., Turpin, B.J., 2005. Isoprene forms secondary organic aerosol through cloud processing:model simulations. Environmental Science & Technology 39, 4441–4446.

Lim, Y.B., Tan, Y., Perri, M.J., Seitzinger, S.P., Turpin, B.J., 2010. Aqueous chemistry and its role in secondary organic aerosol (SOA) formation. Atmos. Chem. Phys. 10, 10521–10539.

Lin, Q., Bi, X., Zhang, G., Yang, Y., Long, P., Lian, X., et al., 2018. In-cloud formation of secondary species in iron-containing particles. Atmospheric Chemistry and Physics Discussions 1–34.

Lin, Q., Yang, Y., Fu, Y., Jiang, F., Zhang, G., Peng, L., et al., 2020. The reductions of oxalate and its precursors in cloud droplets relative to wet particles. Atmos. Environ. 235, 117632.

Meng, J., Wang, G., Li, J., Cheng, C., Cao, J., 2013. Atmospheric oxalic acid and related secondary organic aerosols in Qinghai Lake, a continental background site in Tibet Plateau. Atmos. Environ. 79, 582–589.

Meng, J., Wang, G., Hou, Z., Liu, X., Wei, B., Wu, C., et al., 2018. Molecular distribution and stable carbon isotopic compositions of dicarboxylic acids and related SOA from biogenic sources in the summertime atmosphere of Mt. Tai in the North China Plain. Atmos. Chem. Phys. 18, 15069–15086.

Meng, J., Liu, X., Hou, Z., Yi, Y., Yan, L., Li, Z., et al., 2020. Molecular characteristics and stable carbon isotope compositions of dicarboxylic acids and related compounds in the urban atmosphere of the North China Plain: implications for aqueous phase formation of SOA during the haze periods. Sci. Total Environ. 705, 135256.

Miyazaki, Y., Aggarwal, S.G., Singh, K., Gupta, P.K., Kawamura, K., 2009. Dicarboxylic acids and water-soluble organic carbon in aerosols in New Delhi, India, in winter: characteristics and formation processes. Journal of Geophysical Research: Atmospheres 114, D19206.

Mochizuki, T., Kawamura, K., Miyazaki, Y., Wada, R., Takahashi, Y., Saigusa, N., et al., 2017. Secondary formation of oxalic acid and related organic species from biogenic sources in a larch forest at the northern slope of Mt. Fuji. Atmos. Environ. 166, 255–262.

Moffet, R.C., de Foy, B., Molina, L.T., Molina, M.J., Prather, K.A., 2008. Measurement of ambient aerosols in northern Mexico City by single particle mass spectrometry. Atmos. Chem. Phys. 8, 4499–4516.

Myriokefalitakis, S., Tsigaridis, K., Mihalopoulos, N., Sciare, J., Nenes, A., Kawamura, K., et al., 2011. In-cloud oxalate formation in the global troposphere: a 3-D modeling study. Atmos. Chem. Phys. 11, 5761–5782.

Passananti, M., Vinatier, V., Delort, A.-M., Mailhot, G., Brigante, M., 2016. Siderophores in cloud waters and potential impact on atmospheric chemistry: photoreactivity of iron complexes under sun-simulated conditions. Environmental science & technology 50.

Seinfeld, J., Pandis, S., 1998. Atmospheric Chemistry and Physics: From Air Pollution to Climate Change. vol. 51.

Shahzad, F., Shahzad, U., Fareed, Z., Iqbal, N., Hashmi, S.H., Ahmad, F., 2020. Asymmetric nexus between temperature and COVID-19 in the top ten affected provinces of China: a current application of quantile-on-quantile approach. Sci. Total Environ. 736, 139115.

Sorooshian, A., Lu, M.-L., Brechtel, F.J., Jonsson, H., Feingold, G., Flagan, R.C., et al., 2007a. On the source of organic acid aerosol layers above clouds. Environmental Science & Technology 41, 4647–4654.

Sorooshian, A., Ng, N.L., Chan, A.W.H., Feingold, G., Flagan, R.C., Seinfeld, J.H., 2007b. Particulate organic acids and overall water-soluble aerosol composition measurements from the 2006 Gulf of Mexico Atmospheric Composition and Climate Study (GoMACCS). J. Geophys. Res. 112, D13201.

Wang, G., Kawamura, K., Cheng, C., Li, J., Cao, J., Zhang, R., et al., 2012. Molecular distribution and stable carbon isotopic composition of dicarboxylic acids, ketocarboxylic acids, and α-dicarbonyls in size-resolved atmospheric particles from Xi'an City, China. Environmental Science & Technology 46, 4783–4791.

Wang, G., Cheng, C., Meng, J., Huang, Y., Li, J., Ren, Y., 2015. Field observation on secondary organic aerosols during Asian dust storm periods: formation mechanism of oxalic acid and related compounds on dust surface. Atmos. Environ. 113, 169–176.

Wang, C., Horby, P.W., Hayden, F.G., Gao, G.F., 2020a. A novel coronavirus outbreak of global health concern. Lancet 395, 470–473.

Wang, J., Wang, G., Wu, C., Li, J., Cao, C., Li, J., et al., 2020b. Enhanced aqueous-phase formation of secondary organic aerosols due to the regional biomass burning over North China Plain. Environ. Pollut. 256, 113401.

Weller, C., Tilgner, A., Bräuer, P., Herrmann, H., 2014. Modeling the impact of Iron–carboxylate photochemistry on radical budget and carboxylate degradation in cloud droplets and particles. Environmental Science & Technology 48, 5652–5659.

Wu, Z., Wang, Y., Tan, T., Zhu, Y., Li, M., Shang, D., et al., 2018. Aerosol liquid water driven by anthropogenic inorganic salts: implying its key role in haze formation over the North China plain. Environmental Science & Technology Letters 5, 160–166.

Wu, J., Bei, N., Hu, B., Liu, S., Wang, Y., Shen, Z., et al., 2020. Aerosol–photolysis interaction reduces particulate matter during wintertime haze events. Proc. Natl. Acad. Sci. 117, 9755–9761.

Xu, J., Tian, Y., Cheng, C., Wang, C., Lin, Q., Li, M., et al., 2020a. Characteristics and source apportionment of ambient single particles in Tianjin, China: the close association between oxalic acid and biomass burning. Atmos. Res. 237, 104843.

Xu, K., Cui, K., Young, L.-H., Wang, Y.-F., Hsieh, Y.-K., Wan, S., et al., 2020b. Air quality index, indicatory air pollutants and impact of COVID-19 event on the air quality near Central China. Aerosol Air Qual. Res. 20, 1204–1221.

Yang, F., Chen, H., Wang, X., Yang, X., Du, J., Chen, J., 2009. Single particle mass spectrometry of oxalic acid in ambient aerosols in Shanghai: mixing state and formation mechanism. Atmos. Environ. 43, 3876–3882.

Yu, J.Z., Huang, X.-F., Xu, J., Hu, M., 2005. When aerosol sulfate goes up, so does oxalate: implication for the formation mechanisms of oxalate. Environmental Science & Technology 39, 128–133.

Yu, Q., Chen, J., Qin, W., Cheng, S., Zhang, Y., Ahmad, M., et al., 2019. Characteristics and secondary formation of water-soluble organic acids in PM1, PM2.5 and PM10 in Beijing during haze episodes. Sci. Total Environ. 669, 175–184.

Zhang, G., Lin, Q., Peng, L., Yang, Y., Fu, Y., Bi, X., et al., 2017. Insight into the in-cloud formation of oxalate based on in situ measurement by single particle mass spectrometry. Atmos. Chem. Phys. 17, 13891–13901.

Zhang, G., Lin, Q., Peng, L., Yang, Y., Jiang, F., Liu, F., et al., 2019. Oxalate formation enhanced by Fe-containing particles and environmental implications. Environmental Science & Technology 53, 1269–1277.

Zhao, W., Ren, H., Kawamura, K., Du, H., Chen, X., Yue, S., et al., 2020. Vertical distribution of particle-phase dicarboxylic acids, oxoacids and α-dicarbonyls in the urban boundary layer based on the 325 m tower in Beijing. Atmos. Chem. Phys. 20, 10331–10350.

Zhou, Y., Huang, X.H., Bian, Q., Griffith, S.M., Louie, P.K.K., Yu, J.Z., 2015. Sources and atmospheric processes impacting oxalate at a suburban coastal site in Hong Kong: insights inferred from 1 year hourly measurements. Journal of Geophysical Research: Atmospheres 120, 9772–9788.

Zhu, Y., Yang, L., Chen, J., Kawamura, K., Sato, M., Tilgner, A., et al., 2018. Molecular distributions of dicarboxylic acids, oxocarboxylic acids and α-dicarbonyls in PM2.5 collected at the top of Mt. Tai, North China, during the wheat burning season of 2014. Atmos. Chem. Phys. 18, 10741–10758.

Zou, Y., Charlesworth, E., Yin, C.Q., Yan, X.L., Deng, X.J., Li, F., 2019. The weekday/weekend ozone differences induced by the emissions change during summer and autumn in Guangzhou, China. Atmos. Environ. 199, 114–126.